Assignment of ^{15}N, $^{13}C^{\alpha}$, $^{13}C^{\beta}$, and HN Resonances in an $^{15}N,^{13}C,^{2}H$ Labeled 64 kDa Trp Repressor−Operator Complex Using Triple-Resonance NMR Spectroscopy and ^{2}H-Decoupling

Xi Shan,[†] Kevin H. Gardner,[‡] D. R. Muhandiram,[‡] N. S. Rao,[‡] Cheryl H. Arrowsmith,*[,†] and Lewis E. Kay*[,‡]

Contribution from the Division of Molecular and Structural Biology, Ontario Cancer Institute and Department of Medical Biophysics, University of Toronto, 610 University Avenue, Toronto, Ontario, Canada M5G 2M9, and Protein Engineering Centers of Excellence and Departments of Medical Genetics, Biochemistry and Chemistry, University of Toronto, Toronto, Ontario, Canada M5S 1A8

Received February 26, 1996[⊗]

Abstract: The near complete (>90%) NMR assignment of ^{15}N, $^{13}C^{\alpha}$, $^{13}C^{\beta}$, and HN chemical shifts is presented for a 64 kDa trp repressor−operator complex consisting of two tandem dimers of $^{15}N,^{13}C,>90\%$ ^{2}H labeled trp repressor, unlabeled 22-base-pair DNA, and unlabeled corepressor, 5-methyltryptophan. The DNA sequence employed contains three copies of the palindromic sequence 5′-CTAG-3′, allowing two dimers of trp repressor to bind to each duplex operator DNA. Chemical shift data establish that each subunit within a given dimer in the complex is in a chemically distinct environment, and the pattern of chemical shift differences between subunits provides information regarding interdimer contacts. Because of the large size of the complex, a number of modifications were made to existing enhanced sensitivity triple-resonance correlation experiments which link $^{13}C^{\beta}$, ^{15}N, and HN chemical shifts; the pulse sequences which include these changes are presented. The experiments make use of constant-time chemical shift evolution of the carbon magnetization, resulting in significant improvements in spectral resolution compared to non-constant-time versions of the pulse schemes. An analysis of the utility of the enhanced sensitivity method for recording spectra of high molecular weight deuterated proteins indicates that this approach produces reasonable sensitivity gains for the 64 kDa trp repressor−operator complex studied here.

Introduction

The utility of partial or complete protein deuteration in concert with $^{15}N,^{13}C$ multidimensional NMR techniques has recently been established through studies on a number of $^{15}N,^{13}C,^{2}H$ labeled protein systems.[1−9] However, the idea of using ^{2}H labeling of proteins as a means of improving spectral quality dates back to the late 1960s with the experiments of Crespi et al.[10] and Markley et al.[11] In the late 1980s, the work of LeMaster demonstrated the importance of random fractional deuteration of proteins to aid in the NOE-based sequential assignment of what was then considered to be a rather large protein by NMR standards, *E. coli* thioredoxin (108 residues).[12] To obtain a balance between reduced line widths and reduced sensitivity, LeMaster prepared a 75% deuterium labeled sample of thioredoxin. Torchia et al. demonstrated in the case of the protein Staphylococcal nuclease that extremely high quality HN−HN NOE spectra could be recorded on a sample with complete deuteration of aliphatic/aromatic side chains.[13] Venters and co-workers[14] and Grzesiek et al.[15] have extended this work in the development of four-dimensional ^{15}N-separated NOESY experiments for proteins highly enriched in both ^{15}N and ^{2}H. Jardetzky, Arrowsmith, and co-workers have used a strategy based on selective deuteration to assign the 25 kDa trp repressor[16] molecule. Subsequently these workers used an approach based on deuteration and heteronuclear-edited NMR methods to determine the structure of a ternary 37 kDa complex consisting of trp repressor (trpR), tryptophan, and a 20-base-pair trp operator DNA fragment.[1]

Recently we developed a suite of triple-resonance NMR experiments for the assignment of backbone ^{15}N, $^{13}C^{\alpha}$ and HN resonances as well as the side chain $^{13}C^{\beta}$ carbons in fully $^{15}N,^{13}C$ labeled and fractionally deuterated proteins.[4,5] The methods were demonstrated on an $^{15}N,^{13}C$, ∼70% ^{2}H, 37 kDa trpR complex of a single trpR homodimer bound to a 20-base-pair consensus sequence (Figure 1a). However, genetic and bio-

* To whom correspondence should be addressed.
† Ontario Cancer Institute and Department of Medical Biophysics.
‡ Protein Engineering Centers of Excellence and Departments of Medical Genetics, Biochemistry, and Chemistry.
⊗ Abstract published in *Advance ACS Abstracts,* July 1, 1996.

(1) Zhang, H.; Zhao, D.; Revington, M.; Lee, W.; Jia, X.; Arrowsmith, C. H.; Jardetzky, O. *J. Mol. Biol.* **1994**, *229*, 735.
(2) Grzesiek, S.; Anglister, J.; Ren, H.; Bax, A. *J. Am. Chem. Soc.* **1993**, *115*, 4369.
(3) Kushlan, D. M.; LeMaster, D. M. *J. Biomol. NMR* **1993**, *3*, 701.
(4) Yamazaki, T.; Lee, W.; Revington, M.; Mattiello, D. L.; Dahlquist, F. W.; Arrowsmith, C. H. Kay, L. E. *J. Am. Chem. Soc.* **1994**, *116*, 6464.
(5) Yamazaki, T.; Lee, W.; Arrowsmith, C. H.; Muhandiram, D. R.; Kay, L. E. *J. Am. Chem. Soc.* **1994**, *116*, 11655.
(6) Nietlispach, D.; Clowes, R. T.; Broadhurst, R. W.; Ito, Y.; Keeler, J.; Kelly, M.; Ashurst, J.; Oschkinat, H.; Domaille, P. J.; Laue, E. *J. Am. Chem. Soc.* **1996**, *118*, 407.
(7) Venters, R. A.; Huang, C. C.; Farmer, B. T., II; Trolard, R.; Spicer, L. D.; Fierke, C. A. *J. Biomol. NMR.* **1995**, *5*, 339.
(8) Farmer, B. T., II; Venters, R. A. *J. Am. Chem. Soc.* **1995**, *117*, 4187.
(9) Zhou, M. M.; Ravichandran, K. S.; Olejniczak, E. T.; Petros, A. M.; Meadows, R. P.; Sattler, M.; Harlan, J. E.; Wades, W. S.; Burakoff, S. J.; Fesik, S. W. *Nature* **1995**, *378*, 584.
(10) Crespi, H. L.; Rosenberg, R. M.; Katz, J. J. *Science* **1968**, *161*, 795.
(11) Markley, J. L.; Putter, I.; Jardetzky, O. *Science* **1968**, *161*, 1249.
(12) LeMaster, D. M.; Richards, F. M. *Biochemistry* **1988**, *27*, 142.
(13) Torchia, D. A.; Sparks, S. W.; Bax, A. *J. Am. Chem. Soc.* **1988**, *110*, 2320.
(14) Venters, R. A.; Metzler, W. J.; Spicer, L. D.; Mueller, L.; Farmer, B. T., II. *J. Am. Chem. Soc.* **1995**, *117*, 9592.
(15) Grzesiek, S.; Wingfield, P.; Stahl, S.; Kaufman, J. D.; Bax, A. *J. Am. Chem. Soc.* **1995**, *117*, 9594.
(16) Arrowsmith, C. H.; Pachter, R.; Altman, R. B.; Iyer, S. B.; Jardetzky, O. *Biochemistry* **1990**, *29*, 6332.

S0002-7863(96)00627-0 CCC: $12.00 © 1996 American Chemical Society

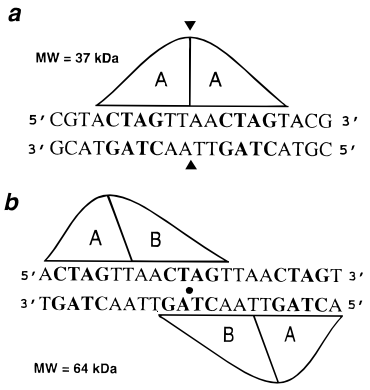

Figure 1. (a) Schematic drawing of the 1:1 trpR−operator complex, 37 kDa, studied previously[1,4,5] and (b) the tandem 2:1 trpR−operator complex, 64 kDa, studied here. The 5′-CTAG-3′ sequences that are most sensitive to mutation in natural operators and which can share two helix−turn−helix DNA-binding motifs[20] in the tandem complex are shown in bold. Each subunit of trpR recognizes the 5′-CT-3′ bases of the 5′-CTAG-3′ sequence.[20] In the 1:1 complex, both subunits are in equivalent chemical environments and therefore have identical chemical shifts. In the 2:1 tandem complex, the two subunits of each dimer are no longer equivalent and have different chemical shifts (A ≠ B). We do not suggest that the structures of the two subunits are significantly different, but only present this diagram to illustrate how the asymmetry in chemical shifts within each dimer arises. The 2-fold axis of symmetry in each of the complexes is indicated.

chemical evidence indicates that multiple trpR dimers bind to natural trp operator sites and that one, two, or three trpR dimers can bind to an operator depending on the sequence and length.[17−19] Therefore, we have recently initiated an NMR study of a 64 kDa complex consisting of two trpR homodimers bound to a symmetrized operator DNA (5′A**CTAG**TTAA**CTAG**T-TAA**CTAG**T3′, see below and Figure 1b) and stabilized by the corepressor analog, 5-methyl-L-tryptophan. A crystal structure of trpR bound in tandem to DNA has recently been published,[20] and on the basis of this structure, it is clear that the axis of symmetry of the complex considered here (see Figure 1b) no longer bisects the trpR dimer, as is the case for the 1:1 complex (Figure 1a). Because of the close contacts between two of the four trpR subunits at the central 5′-CTAG-3′ site and truncation of the DNA near the two flanking 5′-CTAG-3′ sites, the two subunits within each of the dimers are no longer equivalent. As a result, the number of cross peaks observed in spectra recorded on this system is nearly doubled relative to spectra recorded on the 37 kDa, single trpR dimer complex. Analysis of spectra recorded on this tandem dimer system is, therefore, significantly more difficult than for the case of the 37 kDa complex.

In this paper we describe a number of new $^{15}N,^{13}C,^{2}H$-based experiments which are similar to the $^{15}N,^{13}C,^{2}H$ triple-resonance schemes[4,5] that we originally proposed for correlating $^{13}C^{\beta}$, ^{15}N, and HN chemical shifts, but offer significantly improved spectral resolution. The utility of these pulse sequences is demonstrated in the assignment of the backbone resonances of the 64 kDa trpR ternary complex. The backbone $^{15}N,^{13}C^{\alpha}$, HN, and $^{13}C^{\beta}$ chemical shifts are tabulated, and a comparison of the chemical shifts observed for the two unique subunits within each trpR dimer is presented. The high molecular weight of the trpR system has led to an analysis of the efficiency of the enhanced sensitivity[21,22] pulsed field gradient approach[23−25] for recording spectra of large deuterated proteins. To this end the sensitivities of HNCO[26] spectra measured using gradient, sensitivity enhanced and gradient, unenhanced triple-resonance pulse schemes are compared.

Experimental Section

Triply ($^{15}N,^{13}C$, >90% ^{2}H) labeled trpR protein was prepared from the overproducing *E. coli* strain CY15070[27] containing the plasmid pJPR2. The cells were adapted to growth in D_2O using the following scheme. Cells were first grown in M9 media with 200 μg/mL ampicillin and 33% D_2O as the solvent at 37 °C and then plated onto an M9 agar plate made from 33% D_2O. A colony from the 33% plate was used to inoculate M9 media with 56% D_2O, cultured overnight at 37 °C. A frozen stock was prepared from 1 mL of this culture and later plated onto an M9 agar plate made with 99.9% D_2O with sodium acetate as the carbon source instead of glucose. For large-scale purification of triply labeled trpR, a single colony from the 99.9% D_2O/acetate plate was used to inoculate 2 × 25 mL of 99.9% D_2O M9 media with $^{13}CH_3{}^{13}COONa$ and $^{15}NH_4Cl$ as the sole carbon and nitrogen sources, respectively. Following 5 days of growth at 37 °C, each 25 mL culture (OD_{600} = 0.73) was used to inoculate 1 L of the same triply labeled M9 media (1 g/L $^{15}NH_4Cl$, 4 g/L $^{13}CH_3{}^{13}COONa$) containing 10 mL of a mixture of vitamins (100 mL stock solution contains 1 mg of riboflavin, 20 mg of biotin, 10 mg of folic acid, 10 mg of *d*-pantothenate, and 50 mg of thiamin). After an additional 3.2 days of growth the culture reached an absorbance of 0.71 at 600 nm. Subsequently, trpR production was induced by the addition of isopropyl-β-D-thiogalactopyranoside (IPTG) to a concentration of 1 mM. The cells were harvested 18 h later at a final OD_{600} of 1.1. The yield of wet cells was 3.19 g/L. Purification was as described previously[16,27] with an additional elution through a Perceptive Biosystem BioCAD unit. The protein was loaded onto a POROS HQ anion exchange column equilibrated with 12.5 mM sodium phosphate and 12.5 mM NaCl at pH 7.36. The protein was eluted with a gradient of 12.5−400 mM NaCl in the same buffer. The final yield from 2 L of culture was 15 mg of $^{15}N,^{13}C,^{2}H$ labeled trpR which appeared as a single band on a Coomassie Blue stained SDS gel. Mass spectroscopic analysis indicated that the level of deuteration in the protein was 91%.

The protein−DNA complex was prepared by the addition of a one-fourth subunit equivalent of double-stranded synthetic operator (5′-ACTAGTTAACTAGTTAACTAGT-3′) to trpR followed by dialysis and concentration into a pH 6 solution of 10 mM sodium phosphate and a 6.0 mM racemic mixture of 5-methyltryptophan. Only the L-isomer binds with significant affinity to trpR.[28] Final NMR sample conditions were 2.4 mM trpR (monomer), 0.6 mM double-stranded operator DNA, 3.0 mM 5-methyl-L-tryptophan, and 10 mM sodium phosphate adjusted to pH 6, 7% D_2O/93% H_2O, 45 °C.

All experiments were performed on a four-channel Varian UNITY+ 500 MHz spectrometer equipped with a pulsed field gradient unit and an actively shielded triple-resonance probe head. A separate rf channel was used for each of the ^{1}H, ^{13}C, ^{15}N, and ^{2}H pulses. The ^{2}H lock receiver was disabled during application of ^{2}H pulses/decoupling and during field gradient pulses.

The constant-time HNCA experiment (CT-HNCA) was recorded as an 84* × 28* × 512* matrix (the * indicates complex points); acquisition times of 25.7, 23.0, and 64.0 ms in each of t_1, t_2, and t_3 were utilized. The corresponding spectral widths in F_1, F_2, and F_3 were 3268, 1217, and 8000 Hz. The data set was acquired with 16 scans per FID and a repetition delay of 2 s, giving rise to a total acquisition time of 90 h. For the CT-HN(CO)CA experiment, a matrix of 84* × 26* × 512* points was acquired with acquisition times of

(17) Kumamoto, A.; Miller, W.; Gunsalus, R. *Genes Dev*. **1987**, *1*, 556.
(18) Liu, Y. C.; Matthews, K. S. *J. Biol. Chem.* **1993**, *268*, 23239.
(19) Yang, J.; Gunasekera, A.; Lavoi, T. A.; Jin, L.; Lewis, D. E. A.; Carey, J. *J. Mol. Biol.* **1996**, in press.
(20) Lawson, C. L.; Carey, J. *Nature* **1993**, *366*, 178.
(21) Cavanagh, J.; Palmer, A. G.; Wright, P. E.; Rance, M. *J. Magn. Reson.* **1991**, *91*, 429.
(22) Palmer, A. G.; Cavanagh, Wright, P. E. Rance, M. *J. Magn. Reson.* **1991**, *93*, 151.
(23) Kay, L. E.; Keiffer, P.; Saarinen, T. *J. Am. Chem. Soc.* **1992**, *114*, 10663.
(24) Schleucher, J.; Sattler, M.; Griesinger, C. *Angew. Chem., Int. Ed. Engl.* **1993**, *10*, 32.
(25) Muhandiram, D. R.; Kay, L. E. *J. Magn. Reson. B* **1994**, *103*, 203.
(26) Kay, L. E.; Ikura, M.; Tschudin, R.; Bax, A. *J. Magn. Reson.* **1990**, *89*, 496.
(27) Paluh, J. L.; Yanofsky, C. *Nucleic Acids Res.* **1986**, *14*, 7851.
(28) Marmostein, R. Q.; Joachimiak, A.; Sprinzl, M.; Sigler, P. B. *J. Biol. Chem.* **1987**, *262*, 4922.

25.7, 21.4, and 64.0 ms (t_1, t_2, and t_3) and spectral widths of 3268, 1217, and 8000 Hz (F_1, F_2 and F_3). The total measuring time with 16 scans per FID and a repetition delay of 2 s was 84 h. Both the CT-HN(COCA)CB and the CT-HN(CA)CB experiments were acquired with 80* × 28* × 512* complex matrices and with acquisition times of 22.9, 23.0, and 64.0 ms (t_1, t_2, and t_3). Spectral widths of 3500, 1217, and 8000 Hz in F_1, F_2, and F_3 were employed. Each FID was recorded with 16 scans and with a repetition delay of 2.0 s to give total acquisition times of 86 h.

All spectra were processed using nmrPipe/nmrDraw software[29] and analyzed using the program PIPP.[30] In the HN dimension of all data sets a solvent suppression filter[31] was employed to minimize distortions from the residual water signal prior to apodization with a 65°-shifted squared sine-bell window function. The data were subsequently zero filled to twice the size and Fourier transformed, retaining only the downfield half of the spectrum. A 65°-shifted squared sine-bell window function was applied to the carbon dimensions of all the data sets followed by zero filling to 256 complex points, Fourier transformation, phasing, and elimination of the imaginary half of the signal. The size of the ^{15}N time domain was doubled via mirror image linear prediction,[32] apodized using a cosine-bell function, zero filled to 128 complex points, Fourier transformed, and phased, and the imaginaries were eliminated. The absorptive part of each of the 3D data sets from the CT-HNCA, CT-HN(CO)CA, CT-HN(CA)CB, and CT-HN(COCA)CB experiments consisted of 256 × 128 × 512 real points.

In order to assess the efficiency of enhanced sensitivity[21,22] pulsed field gradient methods[23−25] for recording spectra on proteins with high levels of deuteration, a sample of the C-terminal SH2 domain of phospholipase $C_{\gamma 1}$ (PLCC SH2, 105 amino acids) was prepared.[33] Briefly, ^{15}N,^{13}C,^{2}H-labeled PLCC SH2 was generated by overexpression from *E. coli* BL21(DE3) cells transformed with a previously described PLCC clone.[33] Cells were grown at 37 °C in LB media overnight and then transferred into 50 mL of M9 media containing 1 g/L $^{15}NH_4Cl$ and 3 g/L ^{13}C-glucose and grown to $OD_{600} = 0.5$. An aliquot sufficient to start a subsequent culture at $OD_{600} = 0.1$ was centrifuged and resuspended in 50 mL of M9 media in 99.9% D_2O. This growth/centrifuge cycle was repeated two further times with volumes of 100 and 500 mL. Protein expression was induced with 0.25 g/L IPTG and continued at a reduced temperature of 30 °C for 27 h prior to harvesting and cell lysis with sonication. The overexpressed protein was purified with phosphotyrosine affinity chromatography to >95% homogeneity (estimated by Coomassie Blue stained SDS-PAGE), giving a final yield of 15 mg/L. On the basis of mass spectroscopic analysis of similarly prepared ^{14}N,^{12}C,^{2}H samples, the protein is approximately 80% deuterated at aliphatic positions. The lower level of deuteration compared to the trpR case is due to the use of protonated glucose, as opposed to (protonated) acetate, and will lead to decreased amounts of deuteration at specific side chain positions of several amino acid types. Samples were concentrated to ~0.7 mM in a buffer containing 100 mM sodium phosphate (pH 6.0), 0.1 mM EDTA, 0.1 mM DTT, and 0%, 15%, or 30% (volume) glycerol.

HNCO spectra employing the "water flip back" approach[34−36] to minimize saturation/dephasing of water were recorded with (i) the enhanced sensitivity pulse scheme of Figure 1 of ref 34 and (ii) with a "water flip-back water-gate sequence" that does not make use of gradients for coherence transfer selection and does not employ the enhanced sensitivity scheme. Sequence ii is essentially as is illustrated in Figure 1b of ref 25 with the exception that the flip-back approach discussed by Grzesiek and Bax[35] has been added, a number of gradients are included to minimize artifacts and the coherence transfer selection gradients, and g3 and g4, are removed. The correlation time of PLCC SH2 was varied by including either 15% or 30% glycerol in the sample, and spectra were obtained at temperatures of 30, 20, and 10 °C. The correlation time describing the molecular tumbling was estimated for each sample at each of the temperatures by recording backbone ^{15}N T_1, T_2, and steady state ^{1}H−^{15}N NOE experiments and simultaneously fitting all of the data, using procedures described previously.[37] The signal-to-noise values (S/N) of cross peaks were calculated by measuring the peak volumes and dividing by the estimated rms noise intensity obtained from nmrDraw.[29] The S/N of the "enhanced-sensitivity" experiment 1 relative to the "unenhanced" experiment 2 is defined as the ratio $(1/n)\Sigma_k [(S_k/N)_1/(S_k/N)_2]$, where n is the number of cross peaks considered and $(S_k/N)_i$ is the S/N of peak k in experiment i.

Results and Discussion

In a previous publication we have described a number of experiments, CT-HNCA, CT-HN(CO)CA, HN(CA)CB, HN(COCA)CB, and 4D HNCACB, for obtaining backbone assignments of ^{15}N,^{13}C, fractionally ^{2}H labeled proteins.[4,5] The first pair of experiments in the set link HN, ^{15}N and $^{13}C^{\alpha}$ chemical shifts, while the next two experiments correlate HN, ^{15}N, and $^{13}C^{\beta}$ shifts. The 4D HNCACB scheme links HN and ^{15}N, chemical shifts with both intra- and inter-residue ($^{13}C^{\alpha}$,$^{13}C^{\beta}$) pairs. Both CT-HNCA and CT-HN(CO)CA provide spectra with high sensitivity and high resolution. This latter feature is achieved by recording the $^{13}C^{\alpha}$ and the ^{15}N shifts in constant-time mode.[38,39] The use of constant-time (CT) spectroscopy offers significant benefits in terms of resolution for the recording of carbon chemical shifts of proteins. The relatively poor carbon chemical shift dispersion, the presence of substantial one-bond carbon−carbon couplings, and the short carbon transverse relaxation times in protonated proteins significantly degrade the resolution in the carbon dimension of spectra recorded in a non-CT mode. Unfortunately, efficient carbon transverse relaxation often precludes the use of CT-carbon acquisition in triple-resonance experiments recorded on protonated samples. However, the substitution of deuterons for protons at the carbon positions significantly increases the ^{13}C transverse relaxation times (from an average of 16.5 to 130 ms for $^{13}C^{\alpha}$ in the 37 kDa trpR complex), allowing the use of CT spectroscopy with high sensitivity and a significant improvement in resolution.[4,5]

Our previous ^{15}N,^{13}C,^{2}H studies of trpR were conducted on an approximately 70% fractionally deuterated sample with the intent that this NMR sample would be used to carry out both sequential assignments and, subsequently, structural analysis. In constructing this sample we hoped to achieve a reasonable compromise between a sufficiently high level of deuteration with concomitant increase in carbon T_2 values and retaining an adequate supply of protons for the establishment of distance constraints via measurement of ^{1}H−^{1}H NOEs. With this level of deuteration (~70% at the $^{13}C^{\alpha}$ position), high sensitivity spectra can be recorded using CT $^{13}C^{\alpha}$ carbon acquisition. In the case of experiments which record the $^{13}C^{\beta}$ chemical shift, such as the HN(COCA)CB and the HN(CA)CB, cross peaks arise from magnetization which is transferred from $^{13}C^{\alpha}$ to $^{13}C^{\beta}$ and subsequently back to $^{13}C^{\alpha}$ after the $^{13}C^{\beta}$ chemical shift evolution. This process dictates that magnetization reside on the $^{13}C^{\alpha}$ spin in the transverse plane for a time interval of $1/J_{CC}$ (~28 ms), where J_{CC} is the aliphatic one-bond carbon−carbon scalar coupling constant, ~35 Hz. Moreover, if the $^{13}C^{\beta}$ shift is recorded in a constant-time manner, magnetization resides on the β-carbon for an additional ~28 ms. The use of CT-^{13}C spectroscopy for recording $^{13}C^{\beta}$ shift evolution, therefore, requires a high level of deuteration at both α and β positions.

(29) Delaglio, F.; Grzesiek, S.; Vuister, G. W.; Zhu, G.; Pfeifer, J.; Bax, A. *J. Biomol. NMR* **1995**, *6*, 277.
(30) Garrett, D. S.; Powers, R.; Gronenborn, A. M.; Clore, G. M. *J. Magn. Reson.* **1991**, *95*, 214.
(31) Marion, D.; Ikura, M.; Bax, A. *J. Magn. Reson.* **1989**, *84*, 425.
(32) Zhu, G.; Bax, A. *J. Magn. Reson.* **1990**, *90*, 405.
(33) Pascal, S. M.; Singer, A. U.; Gish, G.; Yamazaki, T.; Shoelson, S. E.; Pawson, T.; Kay, L. E.; Forman-Kay, J. D. *Cell* **1994**, *77*, 461.
(34) Kay, L. E.; Xu, G. Y.; Yamazaki, T. *J. Magn. Reson. A* **1994**, *109*, 129.
(35) Grzesiek, S.; Bax, A. *J. Am. Chem. Soc.* **1993**, *115*, 12593.
(36) Stonehouse, J.; Shaw, G., L.; Keeler, J.; Laue, E. *J. Magn. Reson.* A. **1994**, *107*, 178.
(37) Farrow, N. A.; Muhandiram, D. R.; Singer, A. U.; Pascal, S. M.; Kay, C. M.; Gish, G.; Shoelson, S. E.; Pawson, T.; Forman-Kay, J. D.; Kay, L. E. *Biochemistry* **1992**, *33*, 5984.
(38) Santoro, J.; King, G. C. *J. Magn. Reson.* **1992**, *97*, 202.
(39) Vuister, G. W.; Bax, A. *J. Magn. Reson.* **1993**, *101*, 201.

In the case of 70% deuteration this condition is not met, precluding the efficient use of CT spectroscopy for the recording of $^{13}C^{\beta}$ chemical shifts. For this reason the HN(CA)CB and HN(COCA)CB pulse sequences that we developed previously record $^{13}C^{\beta}$ shifts in a non-constant-time manner. The relatively short acquisition times in the carbon dimension in these original experiments, 7−8 ms, limit the resolution available and are a significant problem in the application of the methodology to proteins of increasing size, such as the 64 kDa tandem trpR complex.

Figure 1 provides a comparative illustration of the 37 kDa and the 64 kDa trpR−operator complexes. The presence of an additional 5′-CTAG-3′ site on each DNA strand in Figure 1b allows a second trpR dimer to bind to the complex.[18] Note that, in the tandem dimer (Figure 1b), two of the four trpR subunits interact with each other (molecules labeled "B" in the figure; see discussion below).[20] Each of the subunits within a dimer are, therefore, no longer symmetry related, leading to a near doubling of the numbers of cross peaks in spectra relative to the 37 kDa trpR complex. That is, in the tandem complex, each "A" subunit gives identical spectra which differ from spectra of the identical "B" subunits. The large molecular weight of the tandem trpR complex and especially the approximate 2-fold increase in the number of cross peaks relative to the 37 kDa complex has forced us to reconsider our original strategy of using a 60−70% fractionally deuterated sample for the complete NMR analysis. In the present case we have increased the level of deuteration of the sample so that the $^{13}C^{\beta}$ chemical shift could be recorded in constant-time mode, allowing high-resolution HN(COCA)CB and HN(CA)CB spectra to be obtained. While the minimum level of deuteration necessary for the success of these experiments will likely vary for different proteins, a 90% ^{2}H labeled trpR sample was employed in the experiments described below.

Figure 2 illustrates the CT-HN(COCA)CB (a) and CT-HN-(CA)CB (b) pulse sequences that we have developed. The sequences are similar in many details to their non-constant-time counterparts and are therefore only described briefly here. The flow of magnetization in these experiments can be summarized as follows:

3D CT-HN(COCA)CB

$$\mathrm{HN} \xrightarrow{J_{\mathrm{HN}}} {}^{15}\mathrm{N} \xrightarrow{J_{\mathrm{NC}'}} {}^{13}\mathrm{CO}_{(i-1)} \xrightarrow{J_{\mathrm{C}'\mathrm{C}\alpha}} {}^{13}\mathrm{C}^{\alpha}_{(i-1)} \xrightarrow{J_{\mathrm{C}\alpha\mathrm{C}\beta}} {}^{13}\mathrm{C}^{\beta}_{(i-1)}\,(\mathrm{CT}\ t_1) \xrightarrow{J_{\mathrm{C}\alpha\mathrm{C}\beta}} {}^{13}\mathrm{C}^{\alpha}_{(i-1)} \xrightarrow{J_{\mathrm{C}'\mathrm{C}\alpha}} {}^{13}\mathrm{CO}_{(i-1)} \xrightarrow{J_{\mathrm{NC}'}} {}^{15}\mathrm{N}\,(\mathrm{CT}\ t_2) \xrightarrow{J_{\mathrm{HN}}} \mathrm{HN}\,(t_3)$$

3D CT-HN(CA)CB

$$\mathrm{HN} \xrightarrow{J_{\mathrm{HN}}} {}^{15}\mathrm{N} \xrightarrow{J_{\mathrm{NC}\alpha}} {}^{13}\mathrm{C}^{\alpha} \xrightarrow{J_{\mathrm{C}\alpha\mathrm{C}\beta}} {}^{13}\mathrm{C}^{\beta}\,(\mathrm{CT}\ t_1) \xrightarrow{J_{\mathrm{C}\alpha\mathrm{C}\beta}} {}^{13}\mathrm{C}^{\alpha} \xrightarrow{J_{\mathrm{NC}\alpha}} {}^{15}\mathrm{N}\,(\mathrm{CT}\ t_2) \xrightarrow{J_{\mathrm{HN}}} \mathrm{HN}\,(t_3)$$

The relevant active couplings involved in each transfer step are indicated above the arrows. To emphasize that both the $^{13}C^{\beta}$ and ^{15}N chemical shifts are recorded in constant-time mode, we denote the t_1 and t_2 acquisition times by CT t_1 and CT t_2, respectively. As in the previous family of experiments, pulsed field gradients have been employed to minimize artifacts and residual water in spectra.[40] Additionally, we have employed gradients to select for the coherence transfer pathway with magnetization passing through ^{15}N during the CT t_2 period in each of the sequences, making use of an "enhanced sensitivity pulsed field gradient method".[23−25] An evaluation of the utility of such an approach for application to high molecular weight deuterated proteins is presented below. In these experiments saturation/dephasing of water is kept to a minimum by making use of a strategy that has been described in detail previously.[34−36] It is also noted that improved lock stability can be achieved in these experiments by sandwiching the ^{2}H WALTZ-16$_x$ decoupling element between a 90$_y$,90$_{-y}$ ^{2}H pulse pair[8,41] (i.e., 90$_y$−WALTZ-16$_x$−90$_{-y}$) in a manner analogous to the procedure employed for the minimization of water saturation/dephasing during ^{1}H decoupling applied during pulse schemes recorded on samples dissolved in H_2O.[34] In this way deuterium magnetization is returned to the $+Z$ axis prior to acquisition, ensuring that the lock functions with maximum sensitivity.

The $^{13}C^{\beta}$ chemical shift is recorded in a constant-time manner, during the delay $2T_C$ ($2T_C = 1/J_{CC} \sim 28$ ms) in the sequences of Figure 2a,b. The success of the constant time period in eliminating the effects of the one-bond carbon couplings rests on the fact that aliphatic carbon couplings are relatively uniform in magnitude (∼35 Hz). However, the $^{13}C^{\beta}-^{13}C^{\gamma}$ couplings in the aromatic residues or in Asp/Asn are somewhat larger, $J_{CC} \sim 43-55$ Hz, and in constant-time carbon evolution experiments, with the value of T_C optimized for aliphatic carbon couplings, this difference leads to a net evolution of the aromatic/Asp/Asn $^{13}C^{\beta}$ magnetization. A subsequent decrease in the sensitivity of ($^{13}C^{\beta}$,^{15}N,HN) cross peaks of these residues results. In order to avoid this loss in sensitivity, a G3-inversion pulse[42] is applied at point a in each of the sequences. The excitation profile of this pulse is centered at the midpoint between the carbonyl shifts in Asp and Asn (∼180 ppm) and the aromatic $^{13}C^{\gamma}$ shifts (∼130 ppm), and the pulse is applied with sufficient power that the $^{13}C^{\gamma}$ carbons of the aromatic residues and of Asp/Asn are inverted. The $^{13}C^{\gamma}$ carbons of all other residues are unaffected by this pulse or the subsequent Bloch−Siegert compensation[39] G3-inversion pulse applied immediately prior to the $^{13}C^{\alpha/\beta}$ pulse of phase $\phi 4$ in Figure 2. The application of these pulses ensures that the $^{13}C^{\beta}-^{13}C^{\gamma}$ couplings are refocused at the end of the $2T_C$ period for these residues and there is thus no loss in sensitivity of cross peaks from aromatic or Asp/Asn amino acids. Note that Grzesiek and Bax have exploited the differences in $^{13}C^{\beta}-^{13}C^{\gamma}$ couplings to record ($^{13}C^{\beta}$,$^{1}H^{\beta}$) correlation maps with cross peaks exclusively from aromatic residues or from Asp/Asn.[43]

An additional point of interest in these sequences is that a ^{1}H 180° pulse is applied at a time $\tau_d = 1/(4J_{HC})$ after point a (see Figure 2). This ensures that $^{13}C^{\beta}$ carbons coupled to either one or more protons will not contribute to the observed signal.[4] Note that β-carbon magnetization evolves to give terms which are antiphase with respect to proton magnetization during this interval ($2T_C$) and such terms are not refocused by the subsequent application of pulses in the sequence. The majority of the carbons are completely deuterated and hence will be unaffected by this purging scheme. However, it may well be the case that the protein is not completely deuterated at the β-position and the application of this purge pulse ensures that the resulting spectra are not complicated by additional cross peaks arising from the deuterium isotope shift.[2]

An $^{15}N-HN$ correlation map of the tandem trpR complex is illustrated in Figure 3, showing doubling of many of the cross peaks, as expected from Figure 1. Note, therefore, that while the trpR monomer concentration in the sample employed in the present study is 2.4 mM the "effective" concentration is in fact only 1.2 mM for regions of the molecule showing duplication

(40) Bax, A.; Pochapsky, S. *J. Magn. Reson.* **1992**, *99*, 638.
(41) Muhandiram, D. R.; Yamazaki, T.; Sykes, B. D.; Kay, L. E. *J. Am. Chem. Soc.* **1995**, *117*, 11536.
(42) Emsley, L.; Bodenhausen G. *Chem. Phys. Lett.* **1987**, *165*, 469.
(43) Grzesiek, S.; Bax, A. *J. Biomol. NMR* **1993**, *3*, 185.

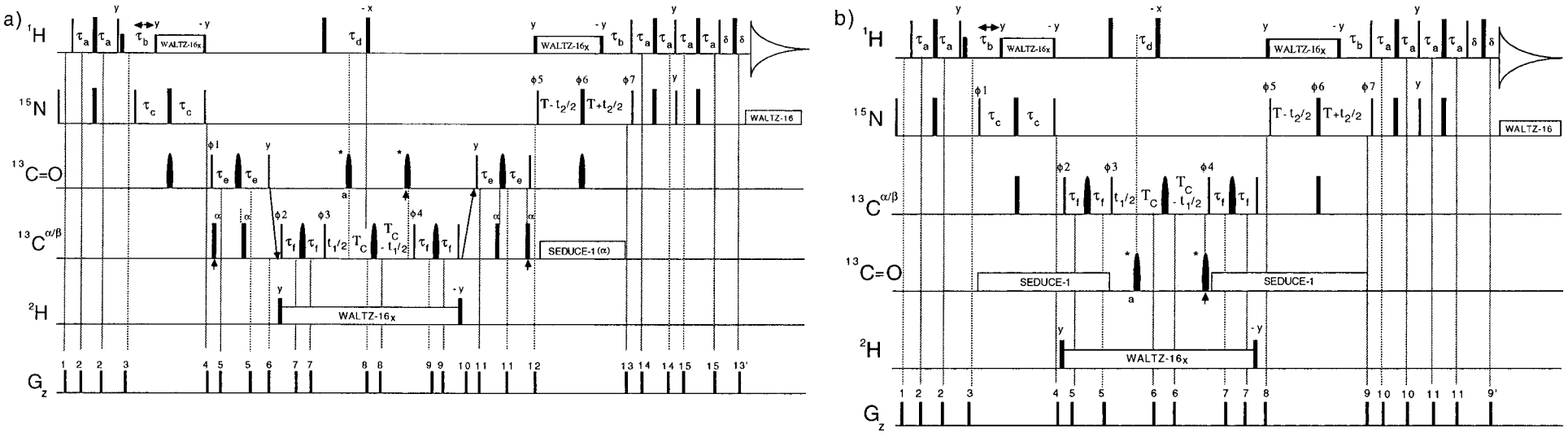

Figure 2. Pulse schemes of the (a) 3D CT-HN(COCA)CB and (b) CT-HN(CA)CB experiments. All narrow (wide) pulses have a flip angle of 90° (180°) and unless indicated otherwise are applied along the x axis. The ^{1}H, ^{15}N, and ^{2}H carriers are centered at 4.6 (water), 119, and 3 ppm, respectively. Proton pulses are applied using a 30 kHz field with the exception of the water-selective 90° pulse during the first INEPT[48] which is a 2 ms rectangular pulse, the 6.8 kHz $\pm y$ pulses flanking the WALTZ-16$_x$[49] decoupling periods, and the 6.8 kHz ^{1}H decoupling periods. All ^{15}N pulses are applied using a 5.8 kHz field, with the exception of ^{15}N decoupling during acquisition which employs a 1 kHz WALTZ-16 decoupling field. All carbon pulses make use of only a single frequency source. The 90$_{\pm y}$ ^{2}H pulses which sandwich the 0.9 kHz ^{2}H WALTZ-16$_x$ decoupling sequence are applied at 2.1 kHz. *All decoupling is interrupted prior to the application of gradient pulses.*[50] Sequence a, CT-HN(COCA)CB: All carbon pulses on the line indicated by ^{13}C═O are applied as "on-resonance" pulses centered at 178 ppm, with the exception of the shaped pulses applied during the constant-time $^{13}C^{\beta}$ evolution period (indicated by *, see below). Carbonyl 180° pulses (first two and last two shaped pulses on ^{13}C═O line) use the SEDUCE-1[51] profile with a length of 230 μs and a peak amplitude of 4.72 kHz. Immediately prior to the $^{13}C^{\alpha/\beta}$ pulse of phase $\phi 2$, the carbon carrier is jumped from 178 to 43 ppm and subsequently jumped back to 178 after the final $2\tau_f$ period. The "diagonal" arrows indicate the positions where the carrier is jumped. The two carbon pulses indicated by * are applied as 370 μs (9.73 kHz at peak amplitude) G3-inversion pulses[42] centered at 150 ppm and invert both carbonyl (C′) and aromatic C$^{\gamma}$ carbons. Because the carbon carrier is at 43 ppm at this point in the sequence these pulses are applied as 107 ppm phase modulated pulses.[52,53] The $^{13}C^{\alpha/\beta}$ 180° pulses marked by α are applied as 120 ppm phase modulated pulses (i.e., center of excitation is at 58 ppm) with an 8.7 kHz field to minimize excitation of C′ spins, while the 90° C′ pulses are applied with a 3.9 kHz field to avoid excitation of $^{13}C^{\alpha}$ magnetization. The 90° $^{13}C^{\alpha/\beta}$ pulses make use of a 4.4 kHz field to minimize excitation of C′ spins. The three shaped $^{13}C^{\alpha/\beta}$ 180° pulses are applied as 400 μs RE-BURP[54] pulses with peak amplitudes of 15.7 kHz and with adjustment of phase so as to compensate for any phase changes that accompany the differences in power used for these pulses and the flanking 90° $^{13}C^{\alpha/\beta}$ pulses. SEDUCE-1 decoupling is applied using a 120 ppm cosine modulated WALTZ-16 field[55] (i.e., centered at 58 ppm) employing pulses having the SEDUCE-1 profile (330 μs 90° pulses). The positions of the Bloch−Siegert compensation pulses[39] are indicated by arrowheads. The delays employed are $\tau_a = 2.4$ ms, $\tau_b = 5.5$ ms, $\tau_c = 12$ ms, $\tau_d = 1.7$ ms, $\tau_e = 4.1$ ms, $\tau_f = 7.0$ ms, $T_C = 14.0$ ms, $T = 12.0$ ms, and $\delta = 0.5$ ms. Note that this timing diagram is not to scale. The ^{1}H 180° pulse of phase $-x$ is applied at a time τ_d after point a. Therefore, there is a delay of $T_C - \tau_d$ between this pulse and the subsequent $^{13}C^{\alpha/\beta}$ RE-BURP pulse. The phase cycling employed is $\phi 1 = (x,-x)$; $\phi 2 = 2(x),2(-x)$; $\phi 3 = 4(y),4(-y)$; $\phi 4 = y$; $\phi 5 = x$; $\phi 6 = 4(x),4(-x)$; $\phi 7 = x$; rec = $(x,-x,-x,x)$. Quadrature in F_1 is achieved via States−TPPI[56] of $\phi 2$ and $\phi 3$. The phase $\phi 5$ and the phase of the receiver are incremented for each distinct value of t_2.[56] Quadrature in F_2 is achieved via the "enhanced sensitivity" PFG method discussed in detail previously.[23−25] The durations and strengths of the gradients (rectangular) are g1 = (0.5 ms, 16 G/cm), g2 = (0.5 ms, 8 G/cm), g3 = (1.0 ms, 20 G/cm), g4 = (1.0 ms, 2G /cm), g5 = (1.0 ms, 14 G/cm), g6 = (1.0 ms, 30 G/cm), g7 = (1.0 ms, 2 G/cm), g8 = (0.150 ms, 16 G/cm), g9 = (0.5 ms, 20 G/cm), g10 = (1.0 ms, 16 G/cm), g11 = (1.0 ms, 1 G/cm), g12 = (0.6 ms, 20 G/cm), g13 = (1.25 ms, 60 G/cm), g13′ = (0.125 ms, 58 G/cm), g14 = (0.5 ms, 3 G/cm), g15 = (0.3 ms, 4 G/cm). Sequence b, CT-HN(CA)CB: Many of the details of this sequence are as described for CT-HN(COCA)CB. Only the differences are indicated here. The carbon carrier is positioned at 43 ppm for the duration of the experiment. All $^{13}C^{\alpha/\beta}$ pulses are applied with a 21 kHz field with the exception of the shaped pulses which are 400 μs RE-BURP[54] pulses with peak amplitudes of 15.7 kHz. As before, the phases of these pulses are adjusted so as to compensate for any changes in phase between the rectangular and shaped pulses that accompany the differences in power levels used. The shaped pulses indicated with * (G3)[42] are centered at 150 ppm and applied as 107 ppm phase-modulated pulses.[52,53] Carbonyl decoupling is achieved by 135 ppm cosine modulation of a WALTZ-16 sequence[49] by employing pulses having the SEDUCE-1 profile[51] (330 μs 90° pulse). As in Figure 1a the timing diagram is not to scale. Note that there is a delay of $T_C - \tau_d$ between the ^{1}H 180° pulse of phase $-x$ and the subsequent $^{13}C^{\alpha/\beta}$ RE-BURP pulse. The phase cycling employed is $\phi 1 = (x,-x)$; $\phi 2 = 2(x),2(-x)$; $\phi 3 = 4(y),4(-y)$; $\phi 4 = y$; $\phi 5 = x$; $\phi 6 = 4(x),4(-x)$, $\phi 7 = x$; rec =$(x,-x,-x,x)$. Quadrature in F_1 and F_2 is achieved in the manner described in a. The durations and strengths of the gradients (rectangular) are g1 = (0.5 ms,16 G/cm), g2 = (0.5 ms, 8 G/cm), g3 = (1.0 ms, 20 G/cm), g4 = (0.5 ms, 16 G/cm), g5 = (0.1 ms, 60 G/cm), g6 = (0.150 ms, 16 G/cm), g7 = (0.10 ms, 60 G/cm), g8 = (0.6 ms, 20 G/cm), g9 = (1.25 ms, 60 G/cm), g9′ = (0.125 ms, 58 G/cm), g10 = (0.5 ms, 3 G/cm), g11 = (0.3 ms, 4 G/cm).

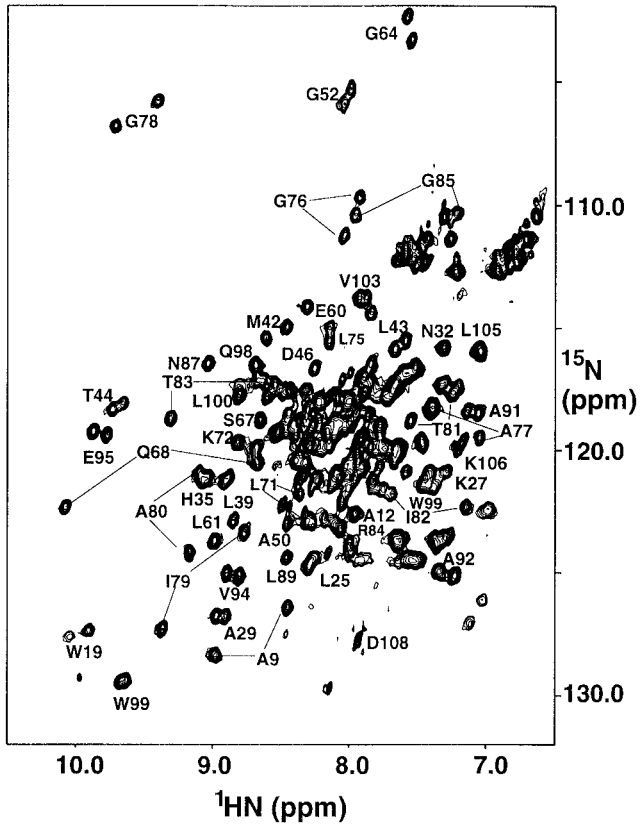

Figure 3. $^{15}N-^{1}H$ correlation map of the 64 kDa tandem trpR complex with selected resonances labeled, illustrating the doubling of cross peaks observed for the majority of the residues.

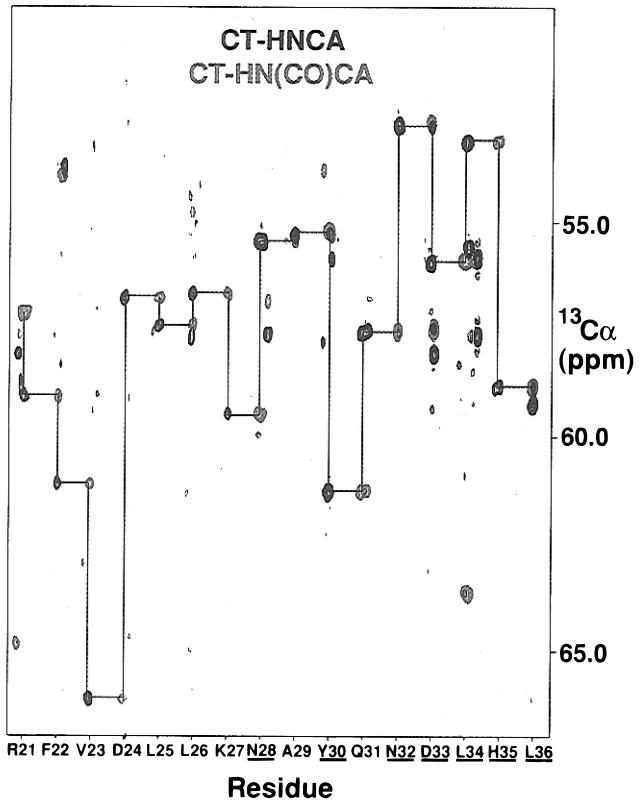

Figure 4. Strip plot showing $^{13}C^{\alpha}(i)/^{13}C^{\alpha}(i-1)$, $^{15}N(i)$, and HN(i) chemical shift correlations extending from Arg 21 to Leu 36 of a single subunit in CT-HNCA (black) and CT-HN(CO)CA (red) spectra. Residues which are underlined have identical $^{13}C^{\alpha}$, ^{15}N, and HN chemical shifts in both subunits of the dimer.

of resonances (∼85% of trpR). Furthermore, the high content of α-helical secondary structure in this protein combined with the doubling of cross peaks results in severe overlap in the central part of the ^{15}N-HN HSQC spectrum. In order to assign the backbone resonances of both the "A" and "B" subunits, we made use of the four constant-time triple-resonance experiments discussed below.

Figures 4−7 illustrate the application of the various triple-resonance pulse schemes that we have developed to obtain the $^{13}C^{\alpha}$,$^{13}C^{\beta}$,^{15}N, and HN assignments of the 64 kDa complex of trpR, 5-methyltryptophan, and the 22-base-pair DNA sequence indicated in Figure 1b. Figure 4 shows a strip plot of data from the CT-HNCA and CT-HN(CO)CA experiments extending from Arg 21 to Leu 36. In this region of the protein, the chemical shift differences between subunits "A" and "B" are small and therefore the connectivity pattern for only a single subunit is shown. In the case of the CT-HN(CO)CA scheme only inter-residue correlations of the form $\{^{13}C^{\alpha}(i-1),^{15}N(i),HN(i)\}$ are observed, while in principle, both intra- and inter-residue correlations linking $^{13}C^{\alpha}$,^{15}N, and HN are obtained in the CT-HNCA experiment. In practice, however, we find that only approximately 37% of the inter-residue correlations are observed in the CT-HNCA experiment (see Gln 31 and Asn 32, for example) for the 64 kDa tandem trpR complex, while over 88% of the expected intra-residue cross peaks are recorded. In the case of the CT-HN(CO)CA experiment, over 88% of the correlations are observed.

In Figure 5, strip plots from the CT-HN(CA)CB and CT-HN(COCA)CB are indicated for residues Arg 21 to Leu 36. The CT-HN(CA)CB experiment correlates both intra- and inter-residue $^{13}C^{\beta}$ chemical shifts with (^{15}N,HN) pairs, while only inter-residue correlations are provided by the CT-HN(COCA)-CB experiment. Approximately 85% of the intra-residue correlations and 27% of the inter-residue connectivities are available from the CT-HN(CA)CB data set, while 87% of the expected cross peaks are observed in the CT-HN(COCA)CB spectrum.

Figures 6 and 7 show strip plots from CT-HNCA/CT-HN-(CO)CA (Figure 6) and CT-HN(CA)CB/CT-HN(COCA)CB (Figure 7) spectra, focusing on the region from Asn 73 to Ala 80. These residues lie within the helix−turn−helix DNA-binding motif. Note that cross peaks for both "A" and "B" subunits can clearly be identified for this region.

The sensitivities of the two new experiments, CT-HN-(COCA)CB and CT-HN(CA)CB, have been quantitated by measuring the signal-to-noise ratio (*S*/*N*) of each cross peak, and the percentage of residues having a defined sensitivity is plotted in Figure 8. A fairly substantial variation in peak intensity is expected on the basis of the 2-fold difference in effective concentration between residues that are or are not doubled. Nevertheless the average values of *S*/*N* for the CT-HN(COCA)CB and CT-HN(CA)CB experiments, ∼20 and 12 (intra-residue correlations), respectively, are relatively high. An average *S*/*N* value of ∼7 for the inter-residue connectivities in the CT-HN(CA)CB was measured, and as indicated above, in many cases, inter-residue correlations were not observed in this experiment. Note that the values reported for *S*/*N* were obtained by excluding the terminal residues, Ala 2−Ala 12 and Trp 99−Asp 108, which give cross peaks of very high intensity.

As discussed previously, the use of CT $^{13}C^{\beta}$ chemical shift evolution greatly improves the resolution available in the carbon dimension of HN(COCA)CB and HN(CA)CB spectra. However, there is an additional benefit in that the sign of the cross peaks can be used in the assignment process. For example, it is straightforward to show that residues with an odd number of *aliphatic* carbons attached to the β-carbon position will give rise to $\{^{13}C^{\beta},^{15}N,HN\}$ correlations of one sign, while residues

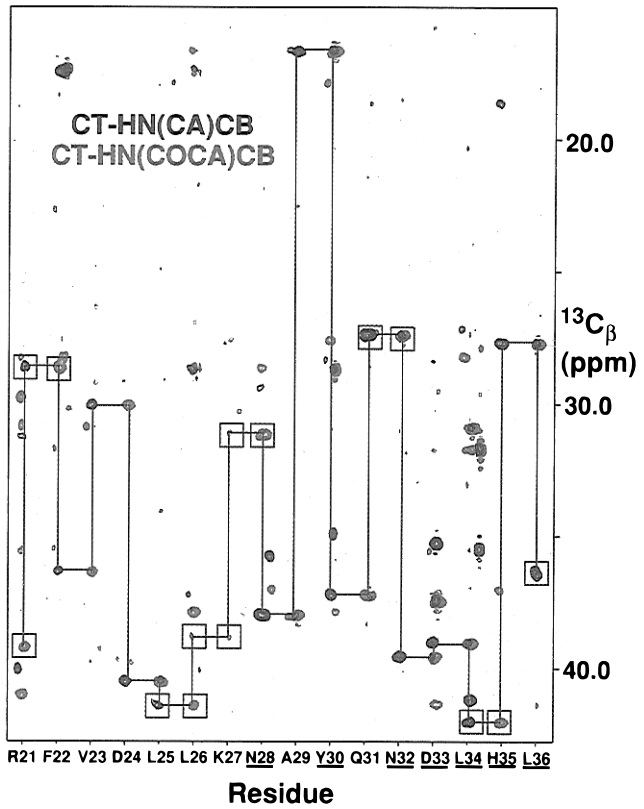

Figure 5. Strip plot of CT-HN(CA)CB (black) and CT-HN(COCA)-CB (red) spectra illustrating $^{13}C^{\beta}(i)/^{13}C^{\beta}(i-1)$, $^{15}N(i)$, and HN(i) correlations extending from Arg 21 to Leu 36. Square boxes indicate cross peaks of negative phase, while residues with identical $^{13}C^{\beta}$, ^{15}N, and HN chemical shifts in both subunits of the dimer are underlined.

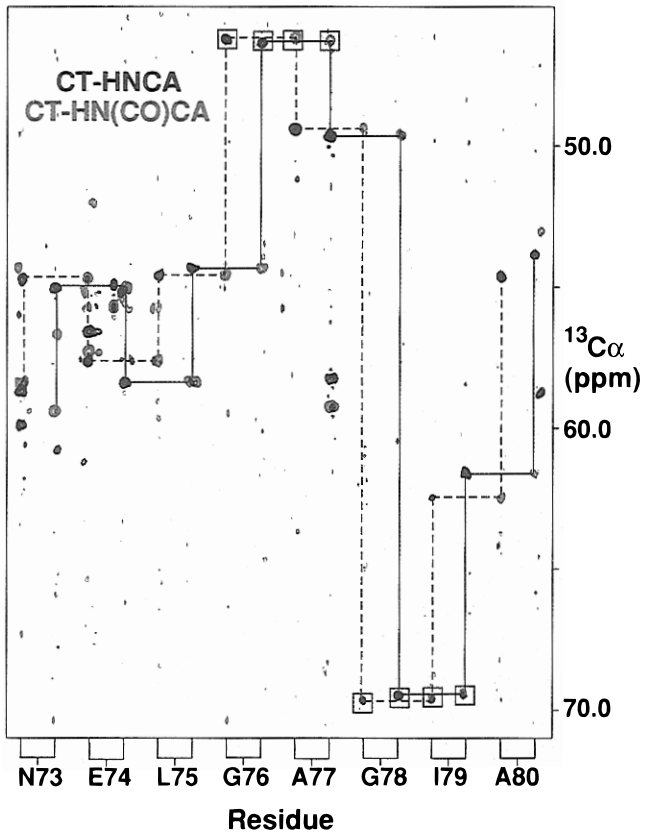

Figure 6. Strip plot of CT-HNCA (black) and CT-HN(CO)CA (red) spectra for residues Asn 73−Ala 80. The solid line shows the inter-residue connectivity within one subunit, and the dashed line shows the connectivity within the other. Peaks that are negative are indicated by the square boxes. Note that the correlations involving Gly 78 are folded once in the $^{13}C^{\alpha}$ dimension.

with $^{13}C^{\beta}$ carbons directly coupled to two *aliphatic* carbons generate cross peaks of opposite phase. Glycine residues also contribute {$^{13}C^{\alpha}$,^{15}N,HN} peaks in these spectra with the same phase properties as cross peaks arising from $^{13}C^{\beta}$ coupled to an odd number of aliphatic carbons. Note that approximately equal numbers of amino acids contain either an odd or an even set of aliphatic carbons attached to the C^{β} position. Montelione and co-workers have commented on the utility of the cross peak phase information of the sort described above in the assignment of side chain correlations in CT-HCC(CO)NH-TOCSY experiments.[44] In the present set of experiments this phase information proved extremely useful as a check of the assignments. For example, consider the stretch of residues extending from Tyr 30 to Leu 36. The intra- and inter-residue correlations are predicted to be of opposite phase for Gln 31, Asn 32, Leu 34, His 35, and Leu 36, with the relative phases of the intra- and interpeaks reversed for Gln 31, Leu 34, and Leu 36 relative to Asn 32 and His 35. In contrast, both intra- and inter-residue correlations will be of the same phase for residues Tyr 30 and Asp 33. Figure 5 shows that this is indeed what is observed.

The assignments of HN, ^{15}N, $^{13}C^{\alpha}$, and $^{13}C^{\beta}$ chemical shifts provided by the CT-HNCA, CT-HN(CO)CA, CT-HN(COCA)-CB, and CT-HN(CA)CB experiments are presented in Table 1. There are several points in each sequence, such as at proline residues, where the sequential connectivities are broken. In the absence of additional data it is not possible to place the assignments of the intervening sequence within an individual subunit. In principle, NOESY data would allow such assignments to be made, assuming that the residues surrounding the break points in the connectivity have different chemical shifts in the two distinct subunits. Unfortunately, the required {i,i+2} and longer range connectivities were not observed in ^{15}N-edited NOE data sets of the tandem trpR complex, precluding subunit-specific assignments. However, even in the absence of information regarding the placement of these sequences within the proper strand, it is possible to compare absolute chemical shift differences between the two subunits ("A" and "B", Figure 1b). Figure 9 illustrates that the largest differences in HN, ^{15}N, $^{13}C^{\alpha}$, and $^{13}C^{\beta}$ chemical shifts arise from residues that are either in the N-terminal portion of the structure (Glu 3−Leu 25) or present in the helix−turn−helix region (Glu 65−Lys 90). Residues which face away from the DNA, Tyr 30−Asn 40 corresponding to the end of helix A and most of helix B, and Glu 95−Asp 108, show, on average, much smaller shift differences. These results are consistent with a recent crystal structure of trpR bound in tandem to DNA, in which two helix−turn−helix DNA binding motifs, one each from adjacent trpR dimers ("B" in Figure 1b), are bound in the major groove of the palindromic 5′-CTAG-3′ site.[20] Protein−protein contacts were seen between adjacent dimers involving residues at the N-terminus and in the DNA binding domain. When interpreted in terms of this crystal structure, the chemical shift differences observed between subunits "A" and "B" arise from protein−protein contacts between the "B" subunits of adjacent dimers at the central 5′-CTAG-3′ site of the operator. In contrast, the helix-turn-helix of the "A" subunit in each of the dimers binds separately to the two outer 5′-CTAG-3′ sites. The "A" subunit is therefore not involved in interdimer contacts. These results suggest that, at least in terms of global features, the solution and X-ray derived structures of the complex are likely to be very similar.

As discussed above, all of the experiments used in the present study have been recorded with the "enhanced sensitivity" pulsed

(44) Tashiro, M.; Rios, C. B.; Montelione, G. T. *J. Biomol. NMR* **1995**, *6*, 211.

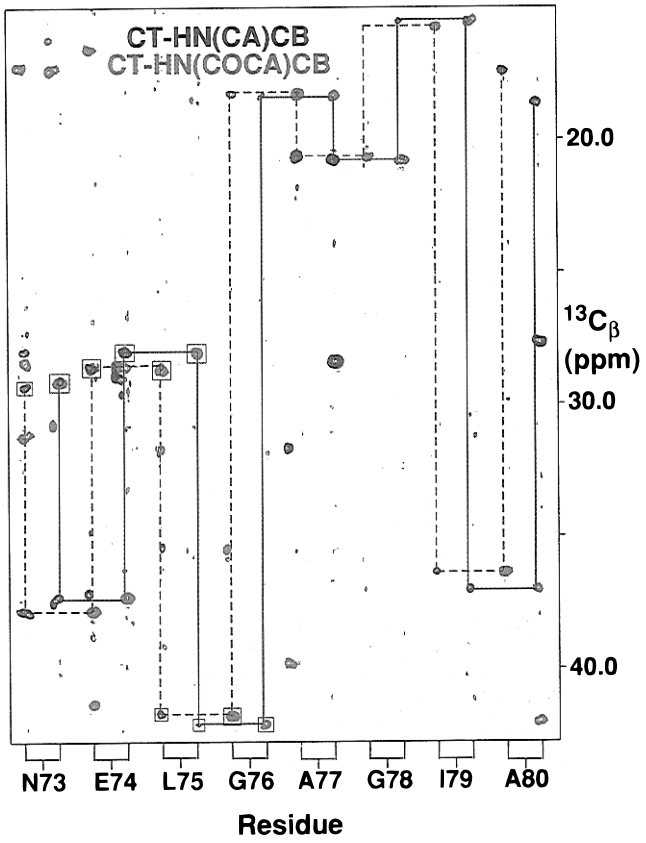

Figure 7. Strip plot of CT-HN(CA)CB (black) and CT-HN(COCA)-CB (red) spectra extending from Asn 73 to Ala 80. Connectivities for the two subunits are distinguished by solid and dashed lines. The square boxes mark the peaks with negative phase.

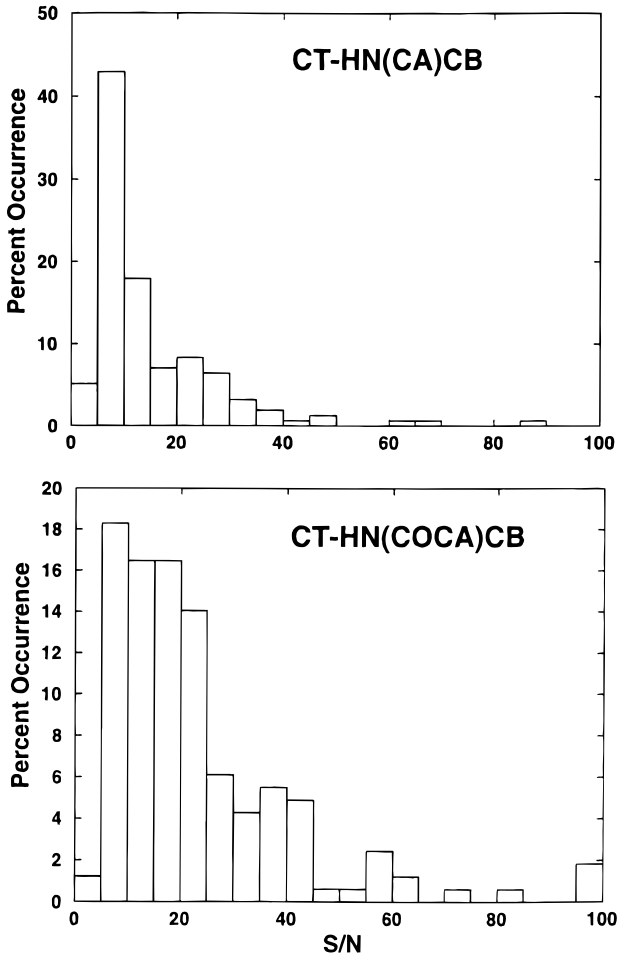

Figure 8. Histograms showing the signal-to-noise (*S*/*N*) of inter-residue correlations in the CT-HN(CO)CACB and intra-residue correlations in the CT-HN(CA)CB. The *S*/*N* of each cross peak was obtained from the peak height using the program PIPP[30] and the rms noise measured using nmrPipe.[29] Overlapped peaks are not included in the histograms, and a number of the peaks from C-terminal residues are off scale (*S*/*N* > 100).

field gradient scheme. In this approach, gradients are applied (13,13′ in CT-HN(COCA)CB, Figure 2a; 9,9′ in CT-HN(CA)-CB, Figure 2b) to select for the coherence transfer pathway with transverse ^{15}N magnetization present during CT t_2 and where the magnetization of interest resides on HN immediately prior to detection. In the absence of relaxation and pulse imperfections the enhanced sensitivity method gives rise to spectra with a $\sqrt{2}$ increase in signal-to-noise over States-[45] or TPPI[46]-type experiments which do not use gradients for transfer pathway selection.[23−25] In practice, sensitivity gains of $\sqrt{2}$ are seldom realized because of the efficient relaxation which occurs in the final portions of such pulse sequences during which time both cosine- and sine-modulated ^{15}N components of magnetization are refocused for detection. Since the rate of relaxation increases with molecular weight it is not clear *a priori* whether the "enhanced sensitivity" methodology is worthwhile for a protein complex the size of the tandem trpR system studied here. Nor is it clear at what molecular weight limit this technique fails to offer advantages, or in fact gives spectra of lower sensitivity, relative to noncoherence transfer selection versions of the experiments. In order to address these questions we prepared an ^{15}N,^{13}C,∼80% ^2H PLCC SH2 sample dissolved in either 0%, 15%, or 30% glycerol. The steep viscosity dependence of glycerol with temperature provides a straightforward approach for manipulating the correlation time of the protein in solution and hence comparing the quality of data obtained on a sample as a function of "effective molecular size". A series of 2D ^{15}N,-HN planes from the "enhanced sensitivity" HNCO[34] and an HNCO scheme that does not employ the sensitivity enhancement method or gradients to select for coherence transfer pathways were recorded as a function of temperature, and the average *S*/*N* of cross peaks in each of the experiments was established, as described in the Experimental Section. Note that both pulse schemes minimized saturation/dephasing of the water resonance using the water flip-back strategy, first described by Grzesiek and Bax.[35] The choice of using the HNCO experiment to evaluate the sensitivities of these two different approaches for recording ^{15}N,HN resolved triple-resonance spectra is based on the excellent sensitivity of this experiment. This allows high-quality data sets to be obtained in reasonable amounts of measuring time. In principle, however, other pulse schemes such as the CT-HNCA or CT-HN(CA)CB could be used. Figure 10 illustrates the enhancements obtained as a function of molecular correlation time for the PLCC SH2 domain. It must be emphasized that the *S*/*N* vs correlation time profile will

(45) States, D. J.; Haberkorn, R. A.; Ruben, D. J. *J. Magn. Reson.* **1982**, *48*, 286.
(46) Marion, D.; Wuthrich, K. *Biochem. Biophys., Res. Commun.* **1983**, *113*, 967.
(47) Zar, Z. H. *Biostatistical Analysis*, 2nd ed., Prentice-Hall: Englewood Cliffs, NJ, 1984.
(48) Morris, G. A.; Freeman, R. *J. Am. Chem. Soc.* **1979**, *101*, 760.
(49) Shaka, A. J.; Keeler, J.; Frenkiel, T.; Freeman, R. *J. Magn. Reson.* **1983**, *52*, 335.
(50) Kay, L. E. *J. Am. Chem. Soc.* **1993**, *115*, 2055.
(51) McCoy, M.; Mueller, L. *J. Am. Chem. Soc.* **1992**, *114*, 2108.
(52) Boyd, J.; Scoffe, N. *J. Magn. Reson.* **1989**, *85*, 406.
(53) Patt, S. L. *J. Magn. Reson.* **1992**, *96*, 94.
(54) Geen, H.; Freeman R. *J. Magn. Reson.* **1991**, *93*, 93.
(55) McCoy, M.; Mueller, L. *J. Magn. Reson.* **1992**, *98*, 674.
(56) Marion, D.; Ikura, M.; Tschudin, R.; Bax, A. *J. Magn. Reson.* **1989**, *85*, 393.
(57) Joachimiak, A.; Kelley, R. L.; Gunsalus, R. P.; Yanofsky, C.; Sigler, P. B. *Proc. Natl. Acad. Sci. U.S.A.* **1983**, *80*, 668.

Table 1. ^{1}HN, ^{15}N, $^{13}C^{\alpha}$, and $^{13}C^{\beta}$ Chemical Shifts for the Tandem Trp Repressor Complex at 45 °C

	subunit 1[a]				subunit 2[a]					subunit 1[a]				subunit 2[a]			
residue[d]	^{1}HN	^{15}N	$^{13}C^{\alpha}$	$^{13}C^{\beta}$	^{1}HN	^{15}N	$^{13}C^{\alpha}$	$^{13}C^{\beta}$	residue[d]	^{1}HN	^{15}N	$^{13}C^{\alpha}$	$^{13}C^{\beta}$	^{1}HN	^{15}N	$^{13}C^{\alpha}$	$^{13}C^{\beta}$
A2[b]									R56	7.36	120.85	58.11	28.24	7.36	121.42	57.35	27.35
E3					8.68	120.14	55.79	28.65	I57	8.32	118.72	65.92	36.79	8.13	118.52	66.13	36.61
E4	8.44	122.37	55.36	28.82	8.49	122.21	55.35	28.69	V58*	8.14	118.99	67.14	30.29	8.14	118.99	67.14	30.29
S5	8.26	118.75	55.75	62.77	8.37	118.69	55.84	62.82	E59	8.32	117.52	59.51	29.01	8.42	118.27	59.81	28.91
P6	—		63.15	30.87	—		(63.32	(31.12)[c]	E60	8.31	114.04	56.83	28.11	8.11	114.88	57.32	28.40
Y7	7.92	119.52	57.49	37.51	(7.84	116.39	56.82	37.03)[c]	L61	8.98	123.68	57.47	39.41	8.85	122.91	57.19	
S8	7.86	117.46	58.05	63.19	7.51	116.43	57.60	63.68	L62	7.88	116.83	56.75	40.88	8.16	119.11	56.47	40.97
A9	8.45	126.36	53.92	17.34	9.00	128.22	54.35	17.53	R63	8.27	119.08	58.77	29.75	8.08	119.24	58.58	29.51
A10	8.07	121.08	53.67	17.42	8.34	120.48	54.35	17.40	G64	7.55	102.31	46.59	—	7.52	103.26	46.14	—
M11	(7.86	118.57	56.39	31.43)[c]	7.68	117.60	56.06	30.78	E65	7.99	118.86	56.66	30.23	7.90	119.44	56.79	29.88
A12	8.06	123.13	54.49	17.40	7.97	122.54	54.66	17.14	M66	8.53	119.12	54.51	34.79	8.25	118.87	55.25	34.01
E13	8.15	119.19	58.34	28.27			(58.18	28.30)[c]	S67	8.66	118.70	57.12	63.55	8.61	117.73	57.07	63.91
Q14	7.94	121.11	58.75	27.49	(8.09	120.92	58.32	27.61)[c]	Q68	10.06	122.24	60.01	25.61	8.68	120.49	59.41	27.31
R15	8.55	117.21	58.03	28.83					R69	8.65	119.94	58.94	28.65	8.09	117.89	58.01	29.10
H16			(58.90	28.24)[c]	(8.32	120.59	59.23	28.41)[c]	E70	7.63	120.18	58.42	28.56	7.63	119.80	58.17	28.87
Q17	(8.31	118.21	58.30	27.22)[c]	8.18	117.84	58.45	27.16	L71	8.29	122.94	57.46	41.01	8.36	121.71	57.17	41.02
E18	(8.39	120.47	58.42	27.45)[c]	8.13	119.92	58.58	27.83	K72	8.82	119.69	59.44	29.27	7.91	120.27	58.69	31.33
W19			59.09	27.56	8.29	122.77	58.65	28.16	N73	7.78	118.99	55.10	37.37	7.63	117.21	54.80	37.93
L20	7.75	117.76	57.10	39.23	8.03	118.12	56.98	39.29	E74	8.22	121.27	58.46	28.12	8.35	119.79	57.70	28.71
R21	7.89	120.64	59.02	28.64	7.71	119.80	58.99	28.62	L75	7.85	114.39	54.39	42.22	8.15	115.51	54.62	41.85
F22	8.11	121.36	61.09	36.38	7.74	120.55	61.42	36.35	G76	8.02	111.09	46.41	—	7.89	109.75	46.37	—
V23	7.77	119.50	66.10	30.08	7.89	119.46	65.93	30.24	A77	7.39	118.46	49.73	20.81	7.06	119.45	49.43	20.69
D24	7.74	121.48	56.75	40.56	8.02	121.59	56.76	40.59	G78	9.40	105.83	43.64	—	9.73	106.79	45.76	—
L25	8.24	124.39	57.38	41.47	7.96	124.14	57.47	41.12	I79	9.34	127.23	61.56	37.10	8.74	123.34	62.46	36.43
L26	8.34	119.93	56.65	38.88			56.60	38.85	A80	9.04	120.86	53.92	18.65	9.14	124.21	54.77	17.45
K27	7.42	120.88	59.44	31.15	7.29	120.86	59.51	31.14	T81	7.54	118.59	65.09	67.51	7.20	117.05	64.59	67.68
N28*	7.57	116.73	55.42	38.06	7.57	116.73	55.42	38.06	I82	7.14	122.14	64.47	35.15	7.68	121.78	64.73	36.83
A29	8.88	126.72	55.27	16.70	8.97	126.74	55.18	16.66	T83	9.29	118.63	66.00	67.54	8.64	117.09	66.19	67.93
Y30*	8.38	119.31	61.28	37.27	8.38	119.31	61.28	37.27	R84	7.82	121.20	59.67		7.97	123.57	59.24	28.67
Q31	7.32	117.29	57.57	27.44	7.28	117.21	57.51	27.43	G85	7.19	110.23	48.44	—	7.96	110.42	48.19	—
N32*	7.30	115.76	52.71	39.62	7.30	115.76	52.71	39.62	S86	8.65	117.03	59.97	62.99	8.48	117.55	60.90	61.87
D33*	7.88	117.57	55.91	39.08	7.88	117.57	55.91	39.08	N87	9.03	116.20	55.41	36.56	8.51	119.30	55.34	36.76
L34*	8.24	118.08	53.11	42.09	8.24	118.08	53.11	42.09	S88								
H35*	9.03	121.08	58.80	27.75	9.03	121.08	58.80	27.75	L89	8.30	124.81	57.61	41.35	8.46	124.28	57.46	41.08
L36*	7.46	119.62	59.24	36.42	7.46	119.62	59.24	36.42	K90	7.82	117.10	59.02	31.87	7.92	118.43	58.60	31.28
P37	—		64.79	29.80	—		64.86	29.85	A91	7.10	118.23	51.21	18.45	7.04	118.41	51.29	18.30
L38*	7.93	120.26	58.03	40.13	7.93	120.26	58.03	40.13	A92	7.36	124.07	49.90	16.92	7.34	123.83	49.68	16.92
L39	8.86	120.99	57.92	40.43	8.91	121.23	57.95	40.30	P93	—		62.04	31.25	—		61.97	31.22
N40	8.06	118.61	54.38	37.29	8.16	118.50	54.39	37.24	V94	8.80	125.07	65.54	30.56	8.89	125.03	65.96	30.60
L41	7.66	120.29	57.90				57.93	41.20	E95	9.75	119.29	59.52	27.27	9.85	119.15	59.50	27.35
M42	8.63	115.22	55.47	31.06	8.44	114.73	55.36	30.82	L96*	7.24	117.65	56.73	40.77	7.24	117.65	56.73	40.77
L43	7.68	115.88	53.49	43.64	7.57	115.50	53.24	44.02	R97	7.84	119.78	60.65	29.00	7.75	118.96	60.85	29.22
T44	9.45	117.52	58.82	66.99	9.66	118.09	58.81	66.66	Q98*	8.68	116.49	58.43	27.65	8.68	116.49	58.43	27.65
P45	—		65.27	30.79	—		(62.91	30.88)[c]	W99	7.45	121.38	61.26	27.77	7.40	121.41	61.25	27.77
D46	8.26	116.54	56.48	38.06	(7.83	119.20	56.91	37.65)[c]	L100*	8.80	117.74	57.09	41.40	8.80	117.74	57.09	41.40
E47									E101*	7.88	117.00	59.34	28.44	7.88	117.00	59.34	28.44
R48	7.62	117.12	59.92		7.51	116.81	59.82	29.37	E102*	7.38	118.17	58.33	28.49	7.38	118.17	58.33	28.49
E49	7.61	117.00	58.80	28.08	7.74	118.01	58.62	28.05	V103	7.92	113.73	63.64	30.94	7.87	113.70	63.64	30.95
A50	8.06	122.08	54.64	16.27	8.35	122.83	54.52	16.31	L104*	8.22	117.88	55.56	41.26	8.22	117.88	55.56	41.26
L51	8.02	118.85	58.02	40.32	7.88	119.14	58.02	39.94	L105*	7.03	115.89	54.54	39.90	7.03	115.89	54.54	39.90
G52	8.01	105.88	46.82	—	8.00	105.14	46.78	—	K106*	7.18	119.78	55.85	31.75	7.18	119.78	55.85	31.75
T53	7.94	120.34	66.13	67.98					S107*	8.15	117.74	57.62	63.42	8.15	117.74	57.62	63.42
R54	8.34	121.07	60.34	29.31	8.19	119.83	60.64		D108*	7.92	127.70	55.11	41.13	7.92	127.70	55.11	41.13
V55	7.86	118.20	66.17	30.34	8.08	118.84	65.77	30.30									

[a] There are several points in each sequence (subunit 1 and 2) where the sequential connectivities are broken (for example at Pro residues, see text). It has not been possible to place the assignments of the intervening sequence within a given subunit. In addition, stretches of sequences surrounded by residues with identical chemical shifts in each chain (e.g., A29) could also not be assigned to specific subunits. Additional sets of peaks for residues E3−E13 have been observed in triple resonance spectra. These peaks may be due to additional conformations of the N-terminal region of the protein. [b] ~90% of the amino-terminal methionine of the original trpR translation product is removed.[57] [c] Tentative assignment. [d] * indicates residues for which the chemical shifts of both chains are identical.

vary from protein to protein and the curve in Figure 10 serves, therefore, only as a guide as to the enhancements that one might expect. While the sensitivity of the "enhanced" approach relative to the "unenhanced" method is less than a full factor of $\sqrt{2}$ even at the smallest of correlation times, this method gives measurable sensitivity gains for molecules with correlation times until at least 20 ns. Analysis of the data using Student's *t* test indicates that at the 95% confidence level enhancements are observed for correlation times less than ~16 ns while at the 80% confidence limit a sensitivity gain is observed for a correlation time of 21 ns. In this context, it is noteworthy that an enhancement factor of 1.08 ± 0.12 was noted for the 64 kDa complex (correlation time of 20.5 ± 1.5 ns at 45 °C) using only peaks corresponding to residues located in the interior of the protein in the analysis. It should be emphasized that the enhancements in triple-resonance experiments are likely to be somewhat larger than in ^{15}N−^{1}HN HSQC based experiments which do not record the ^{15}N chemical shift in a constant-time mode. In this case additional delays must be included during ^{15}N evolution to allow for coherence transfer selection without the introduction of chemical shift evolution.[23] Of course, even in the absence of notable gains in *S*/*N* there are advantages in

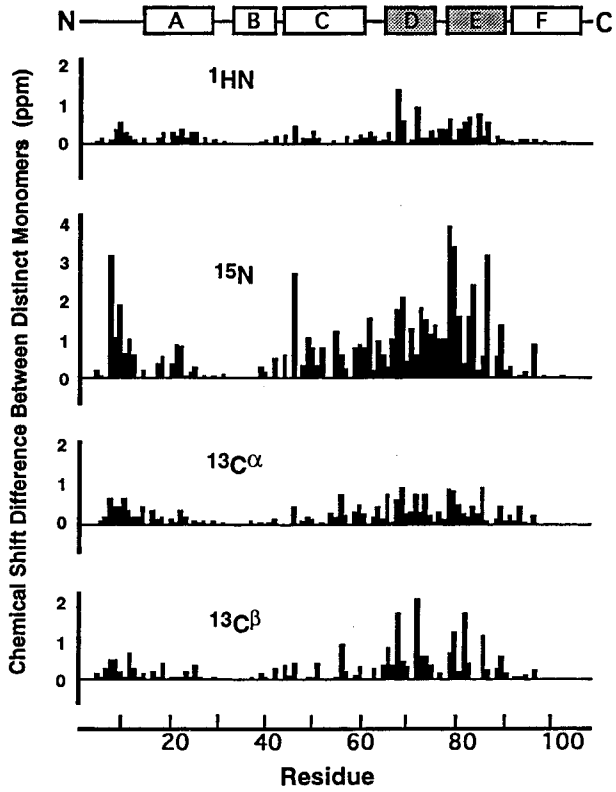

Figure 9. Absolute value of chemical shift differences between the two unique subunits in the tandem trpR complex. Residue number is indicated along the *X* axis, and the absolute value of the difference in chemical shift between the two chains is shown on the *Y* axis for the amide proton, amide nitrogen, α carbon, and *β* carbon. The positions of the six helixes (A−F) of trpR are indicated across the top. Helixes D and E comprise the helix−turn−helix DNA binding motif which contacts the adjacent subunit.

gradient-based coherence transfer selection approaches especially in terms of artifact suppression and the use of minimal phase cycling schemes.[23−25]

Concluding Remarks

In this paper two constant-time triple-resonance experiments are presented for recording the $^{13}C^{\beta}$ chemical shift of $^{15}N,^{13}C,>90\%$ ^2H labeled proteins with high resolution. The experiments have proven extremely useful in the sequential assignment of backbone chemical shifts of a 64 kDa complex consisting of $^{15}N,^{13}C$, >90% ^2H trpR, 5- methyltryptophan and a 22-base-pair trp operator DNA fragment which allows for binding of two trpR dimers per operator. The chemical shifts establish that each subunit within a dimer is no longer equivalent and a near doubling of chemical shifts is observed relative to the 37 kDa complex consisting of one trpR dimer per operator. The results of the present study are consistent with a recently derived X-ray structure of a tandem trpR complex. The differences in chemical shifts between subunits observed in the present study reflect regions of protein−protein contacts between tandem trpR dimers observed in the crystal structure. Since it is necessary to use samples with very high levels of enrichment of ^2H for assignment, it may not be possible to obtain three-dimensional NMR derived solution structures of high molecular weight systems using only a single sample. In the present case, for example, it will be necessary to rely on protein−protein and protein−DNA NOEs obtained from partially protonated samples for the establishment of subunit specific assignments.

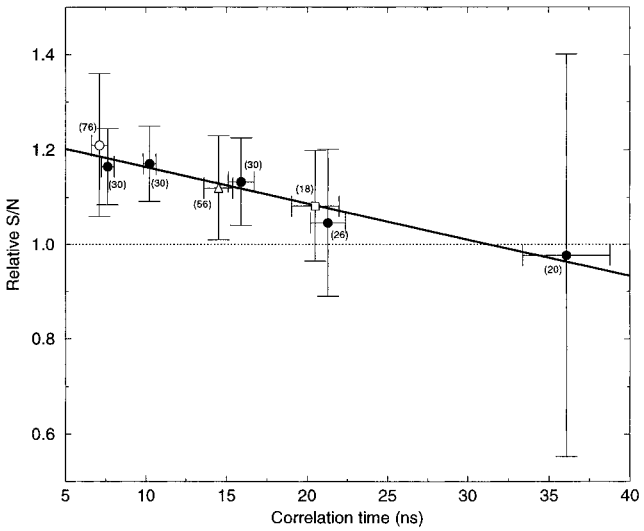

Figure 10. Comparison of the sensitivities of crosspeaks in 2D ^{15}N,-NH planes of HNCO spectra recorded (1) with the enhanced-sensitivity, water flip-back approach[34] and (2) without enhanced sensitivity but with water flip-back.[35] The *S*/*N* of the "enhanced-sensitivity" experiment 1 relative to the "unenhanced" experiment 2 is defined as the ratio $(1/n)\Sigma_k[(S_k/N)_1/(S_k/N)_2]$, where *n* is the number of cross peaks considered and $(S_k/N)_i$ is the *S*/*N* of peak *k* in experiment *i*. The data from PLCC SH2 (105 residues) dissolved in either 100% water ($T = 30$ °C), 15% glycerol (T = 30 °C), or 30% glycerol ($T = 30$, 20, 10 °C) is indicated by ●, while the relative *S*/*N* values for the proteins CheY (14 kDa, ∼80% ^2H, $T = 30$ °C), the 37 kDa trp repressor complex studied previously[4,5] (∼70% ^2H, 37 °C), and the 64 kDa trpR complex described in the present paper are indicated by ○, △, and □, respectively. Note that the CheY and the trp repressor samples were dissolved in water and a temperature study was not performed. The standard deviations in measured values of *S*/*N* and error bars for the derived correlation times are indicated. The number of cross peaks, *n*, used in each *S*/*N* analysis is indicated in brackets adjacent to each of the measured values. The best fit line to the *S*/*N* data from all of the samples is indicated (relative $S/N = -0.077 \times$ correlation time + 1.24, correlation coefficient = 0.97).

Therefore, it may well be the case that different samples will prove optimal at various stages in the structure determination process. Alternatively, samples with high levels of deuterium enrichment at the $^{13}C^{\alpha/\beta}$ positions but retaining sufficient numbers of protons at other positions might prove useful. We are currently pursuing the construction of such samples.

Acknowledgment. This research was supported by the National Cancer Institute of Canada (C.H.A. and L.E.K.), by the Medical Research Council of Canada (C.H.A. and L.E.K.), and by the National Sciences and Engineering Research Council of Canada (L.E.K). K.H.G. is the recipient of an NCI (U.S.) NRSA Fellowship (Grant No. F32 CA68714-01). We acknowledge Cambridge Isotope Laboratories for a gift of $^{13}CH_3{}^{13}CO_2$-Na through their Research Grant Program (C.H.A). The authors thank Professor K. Standing, Dr. L. Donald, and Dr. I. Chernushevich (University of Manitoba) for mass spectroscopic analysis of the trpR sample, Professor R. Dahlquist (University of Oregon) for the gift of the $^{15}N,^{13}C,^2H$ CheY sample, Dr. Steve Pascal (University of Toronto) for assistance in writing the HNCO pulse schemes used in the present analysis, Marees Harris-Brandts (Amgen Institute) for assistance with purification of protein, and Dr. Anchang Shi (Xerox Research Center of Canada) for assistance in making color figures.

JA960627A